Acta Cryst E CRYSTALLOGRAPHIC COMMUNICATIONS

ISSN 2056-9890

Crystal structure, Hirshfeld surface analysis, DFT and molecular docking studies of ethyl 5-amino-2-bromoisonicotinate

Harish Kumar Mahadevaiah,[a] Harishkumar Shivanna,[b] Anil Kumar Hanumaiah,[c] Devarajegowda Hirehalli Chikkegowda[a] and Palakshamurthy Bandrehalli Siddagangaiah[d]*

[a]Department of Physics, Yuvaraja's College, University of Mysore, Mysore, 570005, Karnataka, India, [b]Department of Pharmaceutical Chemistry, Kuvempu University, Shimoga, Karnataka, 577451, India, [c]Department of Physics, Government First Grade College, Chikkabalapura, Karnataka-562101, India, and [d]Department of PG Studies and Research in Physics, Albert Einstein Block, UCS, Tumkur University, Tumkur, Karnataka 572103, India. *Correspondence e-mail: palaksha.bspm@gmail.com

Received 11 October 2024
Accepted 2 November 2024

Edited by S.-L. Zheng, Harvard University, USA

Keywords: crystal structure; Hirshfeld surface; DFT studies; molecular docking; isonicotinate.

CCDC reference: 2395555

Supporting information: this article has supporting information at journals.iucr.org/e

In the title compound, $C_8H_9BrN_2O_2$, the C—O—C—C torsion angle between isonicotine and the ethyl group is 180.0 (2)°. Intramolecular N—H···O and C—H···O interactions consolidate the molecular structure. In the crystal, N—H···N interaction form $S(5)$ zigzag chains along [010]. The most significant contributions to the Hirshfeld surface arise from H···H (33.2%), Br···H/H···Br (20.9%), O···H/H···O (11.2%), C···H/H···C (11.1%) and N···H/H···N (10%) contacts. The topology of the three-dimensional energy frameworks was generated using the B3LYP/6–31 G(d,p) model to calculate the total interaction energy. The net interaction energies for the title compound are E_{ele} = 59.2 kJ mol^{-1}, E_{pol} = 15.5 kJ mol^{-1}, E_{dis} = 140.3 kJ mol^{-1} and E_{rep} = 107.2 kJ mol^{-1} with a total interaction energy E_{tot} of 128.8 kJ mol^{-1}. The molecular structure was optimized by density functional theory (DFT) at the B3LYP/6–311 +G(d,p) level and the theoretical and experimentally obtained parameters were compared. The frontier molecular orbitals HOMO and LUMO were generated, giving an energy gap ΔE of 4.0931 eV. The MEP was generated to identify active sites in the molecule and molecular docking studies carried out with the title compound (ligand) and the covid-19 main protease PDB ID: 6LU7, revealing a moderate binding affinity of −5.4 kcal mol^{-1}.

1. Chemical context

The derivatives of isonicotinate are enantiomerically enriched in the *R* and *S* configuration. The molecules associated with 2-methylalkyl isonicotinate and nicotinate exhibit *R* and *S* configurations at the molecular level. These compounds demonstrate a good anti-fungal activity against different phytopathogenic fungi species and they play significant role in the reduction of the damage at the plant cell and chloroplast levels (Huras *et al.*, 2017). Isonicotinate ligands with an organoruthenium(II) ion form organometallic complexes that exhibit anti-cancer activities (Liu *et al.*, 2012). Silver complexes with nicotinate-based ligands exhibit anti-bacterial activity against clinically isolated pathogens (Abu-Youssef *et al.*, 2007). Various metal complexes with nicotinate moieties have been used to develop phytopathogenic drugs. Most importantly, organotin isonicotinate derivatives are extensively used in the development of antiproliferative drugs, which play a significant role at the innermost layer of cells lining blood vessels and lymphatic vessels (Vieriu *et al.*, 2021). These drugs are used in drug-eluting stents to inhibit vascular smooth muscle cell proliferation possesses, exhibit consider-

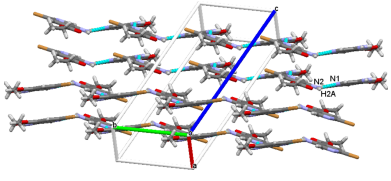

able vasodilator properties and are also used to boost endothelial protective properties (Girgis *et al.*, 2006). The isonicotinate-derived *meso*-tetraarylporphyrin exhibits antioxidant, anti-fungal and allelopathic activities (Dardouri *et al.*, 2024). As part of our studies of this family of materials, we now present the synthesis, structure and Hirshfeld surface analysis of the title compound.

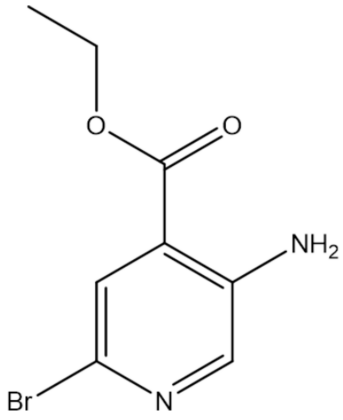

2. Structural commentary

The molecular structure of title compound, which crystallizes in the monoclinic space group *P*21/*c*, is shown in Fig. 1. The amino-2-bromoisonicotinate ring system is essentially planar, with an r.m.s deviation of 0.043 (2) Å. The whole molecule is essentially planar, the dihedral angle between the mean planes defined by the isonocotine moiety and the side chain being 4.30 (2)°. The C6—O1—C7—C8 torsion angle of 175.2 (2)° indicates that the ethyl group is in a planar orientation with the isonocotine ring [see also: C1—C6—O1—C7 = −178.0 (2)° and N2—C2–C1–C6 = −1.2 (4)°]. The molecular

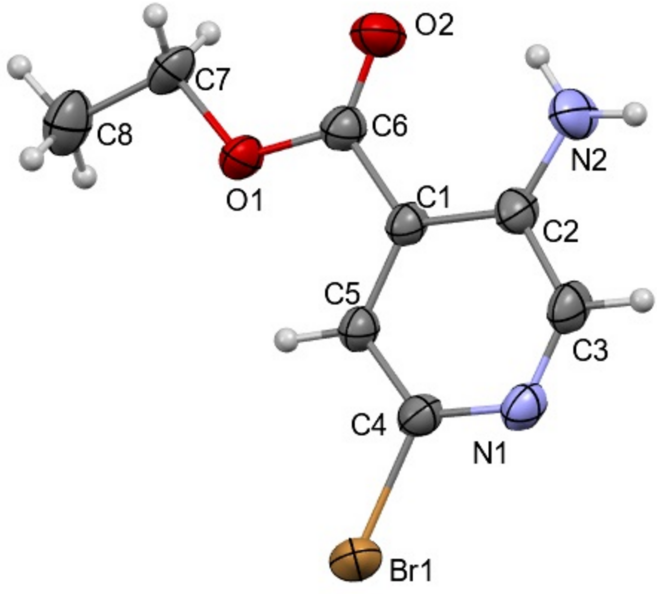

Figure 1
The title molecule with the atom-labeling scheme and 50% probability displacement ellipsoids.

Table 1
Hydrogen-bond geometry (Å, °).

D—H···*A*	*D*—H	H···*A*	*D*···*A*	*D*—H···*A*
N2—H2*B*···O2	0.87 (3)	2.07 (3)	2.746 (3)	133 (2)
C5—H5···O1	0.93	2.37	2.694 (3)	100 (1)
N2—H2*A*···N1^{i}	0.82 (3)	2.30 (3)	3.096 (3)	166 (3)

Symmetry code: (i) $-x, y+\frac{1}{2}, -z+\frac{1}{2}$.

structure is consolidated by N2—H2*B*···O2 and C5—H5···O1 intramolecular interactions (Table 1).

3. Supramolecular features

In the crystal, N2—H2*A*···N1 interactions (Table 1) link the molecules into *S*(5) zigzag chains along [010] as shown in Fig. 2*a* and makes molecular sheets through N—H···N interactions between the four independent molecules in the unit cell, as shown in Fig. 2*b*.

4. Database survey

A search of the Cambridge Structural Database (CSD, version 5.42, update of November 2020; Groom *et al.*, 2016) was undertaken for molecules containing ethyl 3-amino-

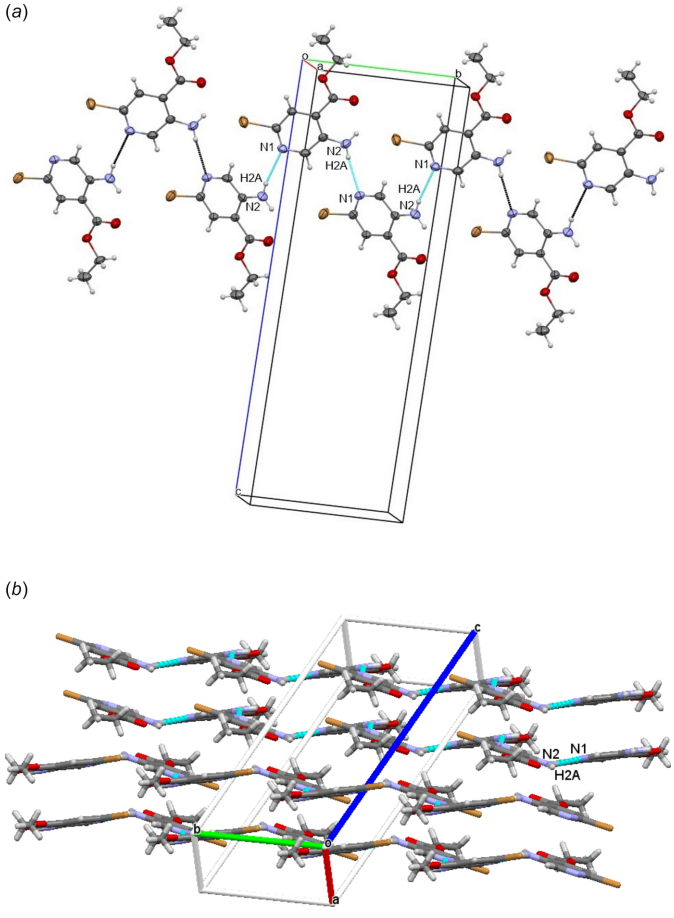

Figure 2
(*a*) The three-dimensional molecular packing of the title compound. Dashed lines indicate N—H···N intermolecular hydrogen bonds forming zigzag chains along [010]. (*b*) Perspective view of the molecular sheets.

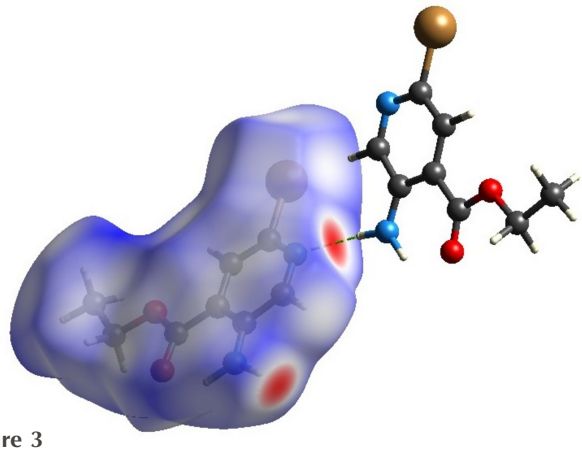

Figure 3
The Hirshfeld surface mapped over d_{norm} with red spots corresponding to the electronegative site of the nitrogen of the molecule.

isonicotinate, 5-amino-2-bromoisonicotinic acid and ethyl 2-bromoisonicotinate fragments, but no hits were found. However, 29 hits were found in a search for molecules containing an ethyl isonicotinate fragment. Among those, in the structures with CSD refcodes ROMMIQ (Wang *et al.*, 2009), SILPOT (Wan *et al.*, 2007), XEZDEM (Han *et al.*, 2007) and XIMBIF (Li *et al.*, 2007), the C—C—O—C torsion angles associated with the isonicotinate are 177.93 (2), −168.46 (3), −168.46 (3) and 176.82 (2)°, respectively, with the same *anti* conformation as in the title compound where the comparable torsion angle is 180.0 (2)°.

5. Hirshfeld surface analysis and interaction energies

CrystalExplorer17.5 (Turner *et al.*, 2017) was used to perform a Hirshfeld surface analysis to quantify the various intermolecular interactions. Fig. 3 illustrates the Hirshfeld surface mapped over d_{norm} with red spots corresponding to electronegative site of the nitrogen through which a short contact N2—H2*A*···N1 forms a hydrogen-bonded chain. The fingerprint plots in Fig. 4 indicate that the major contributions to the Hirshfeld surface of the crystal structure are from H···H (33.2%), Br···H/H···Br (20.9%), O···H/H···O (11.2%), C···H/H···C (11.1%) and N···H/H···N (10%) contacts. The characteristic spikes in the N···H/H···N plot indicate the presence of the N2—H2*A*···N1 hydrogen bond listed in Table 1. The three-dimensional interaction energy between the molecules of the title compound were computed using the basis set B3LYP/6-31G(d,p). The net interaction energies are E_{ele} = 59.2 kJ mol^{-1}, E_{pol} = 15.5 kJ mol^{-1}, E_{dis} = 140.3 kJ mol^{-1}, E_{rep} = 107.2 kJ mol^{-1} with a total interaction energy E_{tot} of128.8 kJ mol^{-1}. The topology of the energy frameworks along the *a*, *b* and *c* axes for the different contributions (Coulombic energy, dispersion energy and total energy) are shown in Fig. 5.

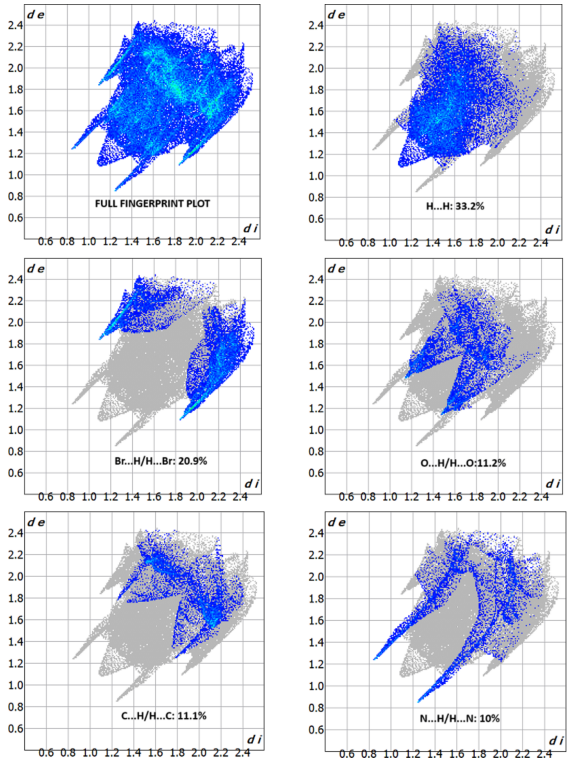

Figure 4
The fingerprint plots of the title molecule, showing the major contributions to the Hirshfeld surface from H···H (33.2%), Br···H/H···Br (20.9%), O···H/H···O (11.2%), C···H/H···C (11.1%) and N···H/H···N (10%) contacts.

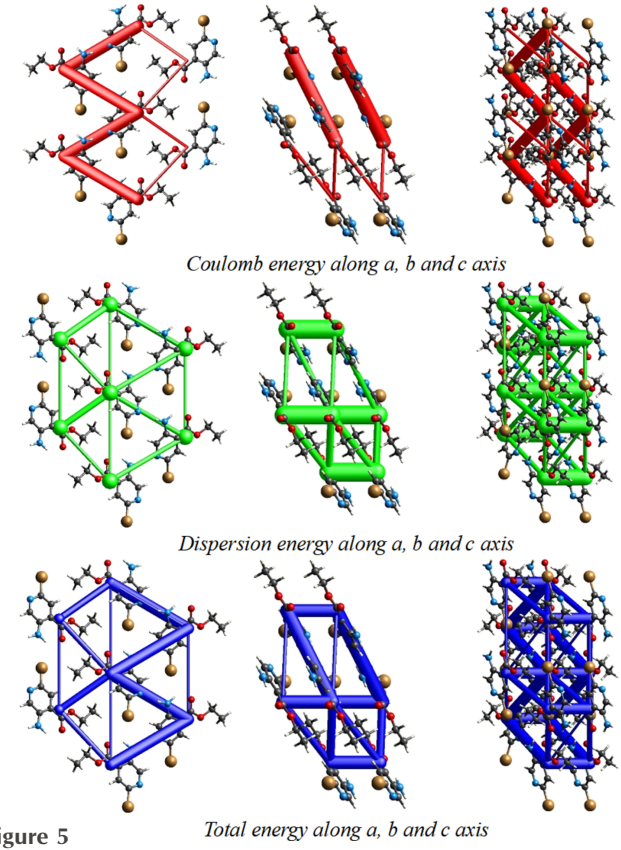

Figure 5
The topology of the energy frameworks along the *a*, *b* and *c* axes for interaction energies.

Table 2
Selected bond lengths, angles and torsion angles (Å, °).

Parameter	SCXRD	DFT
Br1—C4	1.903 (2)	1.9253
O1—C6	1.335 (3)	1.3573
O1—C7	1.454 (3)	1.4551
N2—C2	1.354 (3)	1.3704
C3—N1	1.318 (3)	1.3228
N1—C4	1.327 (3)	1.3226
C6—O1—C7	117.00 (2)	116.13
N2—C2—C1	124.5 (2)	124.95
N2—C2—C3	119.3 (2)	118.77
C2—C3—N1	125.1 (2)	124.62
Br1—C4—N1	116.65 (15)	117.07
Br1—C4—C5	119.19 (16)	119.44
O1—C6—O2	123.0 (2)	122.35
C7—O1—C6—O2	−0.6 (4)	−0.34
C7—O1—C6—C1	180.0 (2)	179.93
C3—N1—C4—Br1	178.8 (2)	179.84
N2—C2—C3—N1	−179.0 (3)	−177.72

6. DFT Studies

The title compound was studied by DFT calculations in the gas phase at the B3LYP/6-311+G(d,p) level of theory with *Gaussian 09W* (Frisch *et al.*, 2009). *GaussView 5.0* was used to generate the optimized molecular structure (Fig. 6). The optimized bond parameters obtained are in good correlation with those obtained from SCXRD analysis (Table 2). The small deviations observed may be attributed to the gas phase (theoretical calculations) compared to the solid phase of SCXRD analysis. The calculated energies of the frontier molecular orbitals are −6.2700 eV and −2.1769 eV. The energy gap ΔE was found to be 4.0931 eV (Fig. 7). The reactivity descriptors calculated from the energy gap value, ionization energy (I), electron affinity (A), electronegativity (χ), chemical hardness (η), chemical potential (μ), electrophilicity index (ω) and chemical softness (S) are 6.2700, 2.1769, 4.2234, 2.0465, −4.2234, 4.3580 eV and 0.2440 eV^{-1} respectively.

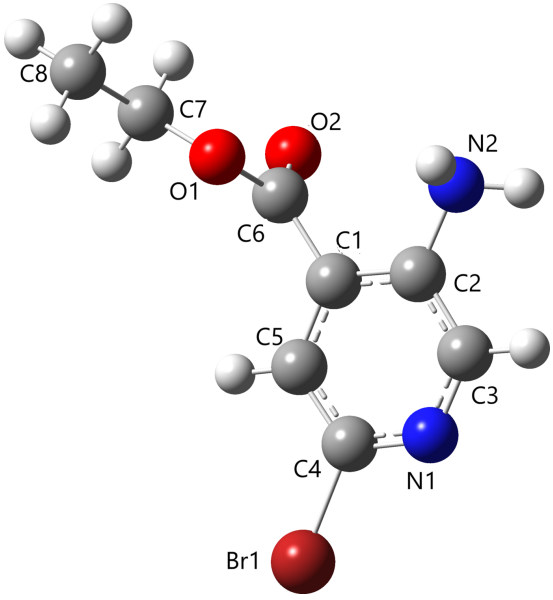

Figure 6
The optimized molecular structure of the title compound generated using *Gaussian 09W*.

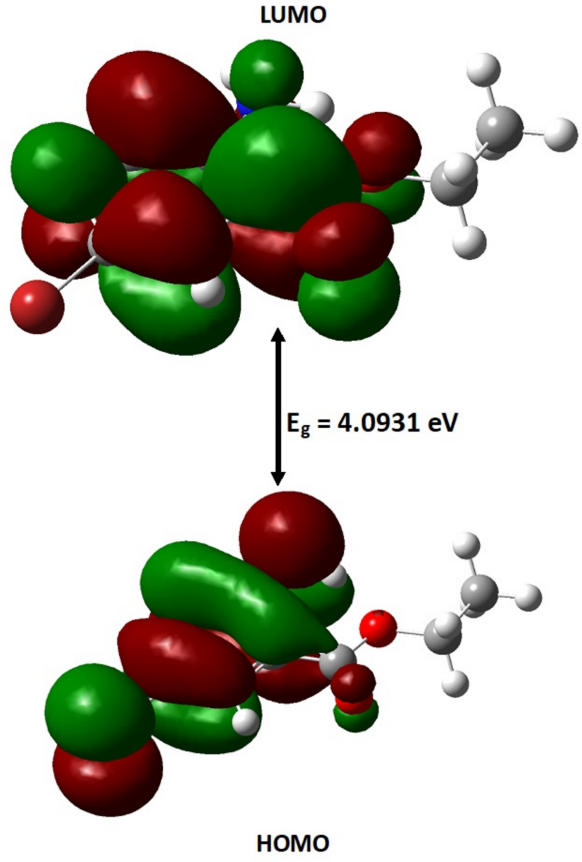

Figure 7
The frontier molecular orbitals HOMO and LUMO energy levels, with the energy gap ΔE = 4.0931 eV.

The MEP surface of the optimized structure of the title compound is depicted in Fig. 8. Nucleophilic and electrophilic reactive sites of the molecule are represented by red- and blue-colored regions on the MEP surface. In the MEP surface of the title compound, the pale red color covering the oxygen and nitrogen atoms of the isonicotinate fragment and the pale-

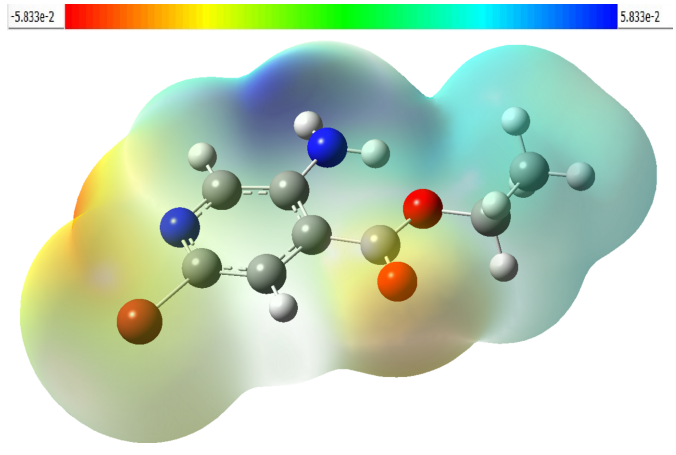

Figure 8
The MEP surface of the optimized molecular structure of the title compound.

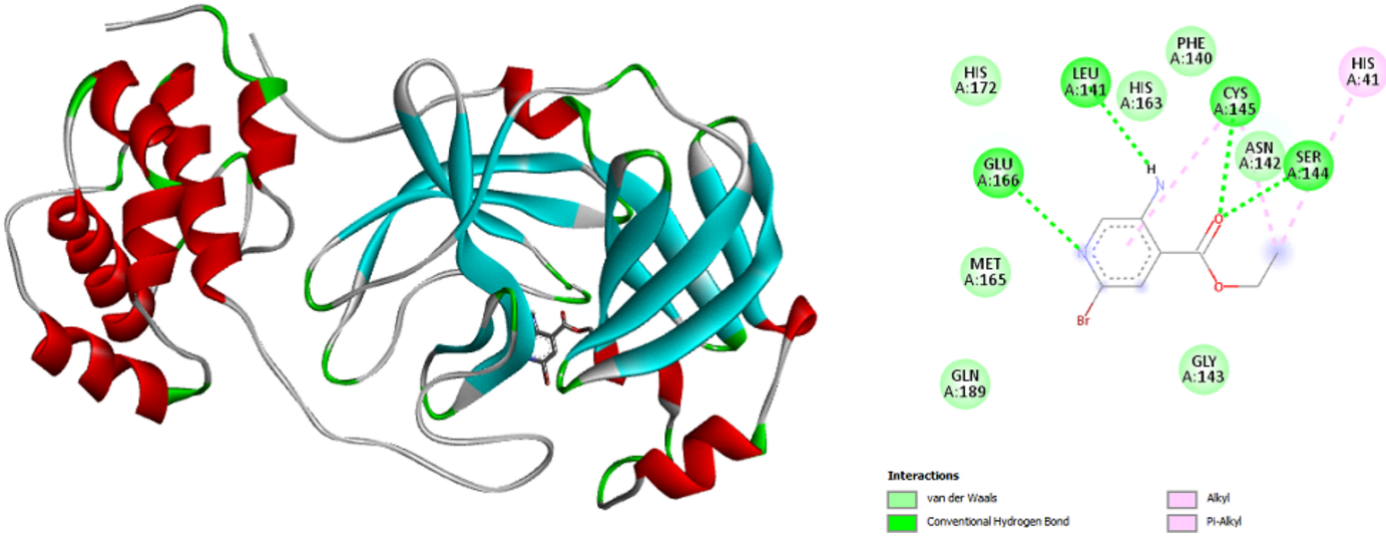

Figure 9
A graphical view of the three-dimensional and two-dimensional docking between the ligand and the receptor protein (covid-19 main protease).

blue color over the amino group are active sites for nucleophilic and electrophilic attack, respectively.

7. Molecular docking studies

The interaction of the ligand with the target receptor, covid-19 main protease (PDB ID: 6LU7) was performed using *Autodock Vina 4.2* (Morris *et al.*, 2009) software. *Biovia Discovery Studio* (Biovia, 2017) was used for visualizing the interactions present between ligand and receptor. The docking results of the ligand with the receptor protein reveal that the ligand has a good binding affinity of −5.4 kcal mol^{-1} and the 2D interaction view shows conventional hydrogen bonding of GLU A:166, LEU A:141, CYS A:145 and SER A:144 with nitrogen and oxygen atoms, van der Waals interactions between the HIS A:163, ASN A:142 amino residues and ethyl −5-amino −2-bromoisonicotinate, Fig. 9. The binding affinity of the title compound with the receptor protein (covid-19 main protease) suggests it to be a potential candidate for pharmaceutical applications. Meanwhile, we have gone through the literature in order to study the efficiency of the title ligand. The docking results of imidazole-anchored azo-imidazole derivatives with the 6LU7 receptor also exhibit a binding affinity of −5.4 kcal mol^{-1} (Chhetri *et al.*, 2021)

8. Synthesis and crystallization

To a stirred a solution of ethyl 3-aminoisonicotinate (800 mg, 1.0 eq) in DMF (8 mL), *N*-bromosuccinimide (NBS; 0.937 mg. 1.1 eq) was added, and the reaction mixture was stirred at room temperature for 6 h. The reaction was monitored by TLC (30% EA: hexane) and it confirmed that the reaction was complete. The reaction mixture was then quenched with water and extracted into ethyl acetate. The organic layer was separated and concentrated to obtain the crude product and purified through Combi-Flash chromatography using 30% EA. Hexane–ethyl acetate was used as mobile phase to obtain the pure compound as a pale-yellow crystal, yield: 98%. A suitable single crystal was used to collect the X-ray data.^{1}H NMR (500 Hz) in $CDCl_3$, δ 7.96 (*s*, 1H, Ar-H), 7.78 (*s*, 1H, Ar-H), 5.69 (*s*, 2H, NH_2), 4.36 (*t*, *J* = 7 Hz, 2H, OCH_2^-), 1.42 (*t*, *J* = 7 Hz, 3H, $-CH_3$) ppm. ^{13}C NMR, 125 Hz: δ 165.8, 144.1, 140.3, 126.9, 118.8, 61.6, 14.2 ppm.

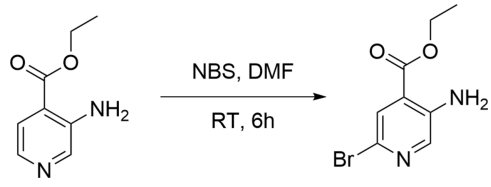

9. Refinement

Crystal data, data collection and structure refinement details are summarized in Table 3. The hydrogen atoms attached to N were located in difference maps. The distances H2*A*/H2*B*—N2 were restrained to 0.82 (2) Å. All other H atoms were positioned with idealized geometry and refined using a riding model with C—H = 0.93–0.97 Å and U_{iso}(H) = 1.2U_{eq}(C) or 1.5U_{eq}(methyl C).

Acknowledgements

HM extends his gratitude to Kishore and Shashikanth SSCU, IISc for their help in collecting the SCXRD data.

Funding information

Funding for this research was provided by: Vision Group of Science and Technology, Government of Karnataka (award No. GRD319 to Palakshamurthy Bandrehalli Siddagangaiah).

References

Abu-Youssef, M. A., Dey, R., Gohar, Y., Massoud, A. A. A., Öhrström, L. & Langer, V. (2007). *Inorg. Chem.* **46**, 5893–5903.

Biovia (2017). *Discovery Studio Visualizer*. Biovia, SanDiego, CA, USA.

Bruker (2014). *APEX2* and *SAINT*. Bruker AXS Inc., Madison, Wisconsin, USA.

Chhetri, A., Chettri, S., Rai, P., Mishra, D. K., Sinha, B. & Brahman, D. (2021). *J. Mol. Struct.* **1225**, 129230.

Dardouri, N. E., Hrichi, S., Torres, P., Chaâbane-Banaoues, R., Sorrenti, A., Roisnel, T., Turowska-Tyrk, I., Babba, H., Crusats, J., Moyano, A. & Nasri, H. (2024). *Molecules*, **29**, 3163.

Frisch, M. J., Trucks, G. W., Schlegel, H. B., Scuseria, G. E., Robb, M. A., Cheeseman, J. R., Scalmani, G., Barone, V., Mennucci, B., Petersson, G. A., Nakatsuji, H., Caricato, M., Li, X., Hratchian, H. P., Izmaylov, A. F., Bloino, J., Zheng, G., Sonnenberg, J. L., Hada, M., Ehara, M., Toyota, K., Fukuda, R., Hasegawa, J., Ishida, M., Nakajima, T., Honda, Y., Kitao, O., Nakai, H., Vreven, T., Montgomery, J. A. Jr, Peralta, J. E., Ogliaro, F., Bearpark, M., Heyd, J. J., Brothers, E., Kudin, K. N., Staroverov, V. N., Kobayashi, R., Normand, J., Raghavachari, K., Rendell, A., Burant, J. C., Iyengar, S. S., Tomasi, J., Cossi, M., Rega, N., Millam, J. M., Klene, M., Knox, J. E., Cross, J. B., Bakken, V., Adamo, C., Jaramillo, J., Gomperts, R., Stratmann, R. E., Yazyev, O., Austin, A. J., Cammi, R., Pomelli, C., Ochterski, J. W., Martin, R. L., Morokuma, K., Zakrzewski, V. G., Voth, G. A., Salvador, P., Dannenberg, J. J., Dapprich, S., Daniels, A. D., Farkas, O., Foresman, J. B., Ortiz, J. V., Cioslowski, J. & Fox, D. J. (2009). *Gaussian 09W*, Revision A. 02. Gaussian, Inc., Wallingford CT, USA.

Girgis, A. S., Kalmouch, A. & Ellithey, M. (2006). *Bioorg. Med. Chem.* **14**, 8488–8494.

Groom, C. R., Bruno, I. J., Lightfoot, M. P. & Ward, S. C. (2016). *Acta Cryst.* B**72**, 171–179.

Han, X.-J., Zeng, W.-L., Bi, S. & Wan, J. (2007). *Acta Cryst.* E**63**, o1194–o1195.

Huras, B., Zakrzewski, J., Krawczyk, M., Bombińska, D., Cieniecka-Rosłonkiewicz, A. & Michalczyk, A. (2017). *Med. Chem. Res.* **26**, 509–517.

Krause, L., Herbst-Irmer, R., Sheldrick, G. M. & Stalke, D. (2015). *J. Appl. Cryst.* **48**, 3–10.

Li, J., Zeng, W.-L., Wang, M.-H. & Wan, J. (2007). *Acta Cryst.* E**63**, o4177.

Liu, K. G., Cai, X. Q., Li, X. C., Qin, D. A. & Hu, M. L. (2012). *Inorg. Chim. Acta*, **388**, 78–83.

Macrae, C. F., Sovago, I., Cottrell, S. J., Galek, P. T. A., McCabe, P., Pidcock, E., Platings, M., Shields, G. P., Stevens, J. S., Towler, M. & Wood, P. A. (2020). *J. Appl. Cryst.* **53**, 226–235.

Table 3
Experimental details.

Crystal data	
Chemical formula	$C_8H_9BrN_2O_2$
M_r	245.08
Crystal system, space group	Monoclinic, $P2_1/c$
Temperature (K)	567
a, b, c (Å)	4.1538 (9), 8.9978 (16), 25.487 (5)
β (°)	92.468 (7)
V (Å^3)	951.7 (3)
Z	4
Radiation type	Mo $K\alpha$
μ (mm^{-1})	4.29
Crystal size (mm)	0.32 × 0.27 × 0.21
Data collection	
Diffractometer	Bruker SMART APEXII CCD
Absorption correction	Multi-scan (*SADABS*; Krause *et al.*, 2015)
T_{min}, T_{max}	0.225, 0.401
No. of measured, independent and observed [$I > 2\sigma(I)$] reflections	21643, 2353, 1910
R_{int}	0.037
(sin $\theta/\lambda)_{max}$ (Å^{-1})	0.666
Refinement	
$R[F^2 > 2\sigma(F^2)]$, $wR(F^2)$, S	0.032, 0.069, 1.04
No. of reflections	2353
No. of parameters	126
H-atom treatment	H atoms treated by a mixture of independent and constrained refinement
$\Delta\rho_{max}$, $\Delta\rho_{min}$ (e Å^{-3})	0.53, −0.45

Computer programs: *APEX2* and *SAINT* (Bruker, 2014), *SHELXT2018/2* (Sheldrick, 2015*a*), *SHELXL2019/2* (Sheldrick, 2015*b*) and *Mercury* (Macrae *et al.*, 2020).

Morris, G. M., Huey, R., Lindstrom, W., Sanner, M. F., Belew, R. K., Goodsell, D. S. & Olson, A. J. (2009). *J. Comput. Chem.* **30**, 27852791.

Sheldrick, G. M. (2015*a*). *Acta Cryst.* A**71**, 3–8.

Sheldrick, G. M. (2015*b*). *Acta Cryst.* C**71**, 3–8.

Turner, M. J., MacKinnon, J. J., Wolff, S. K., Grimwood, D. J., Spackman, P. R., Jayatilaka, D. & Spackman, M. A. (2017). *CrystalExplorer17.5*. University of Western Australia. http://crystalexplorer.net.

Vieriu, S. M., Someşan, A. A., Silvestru, C., Licarete, E., Banciu, M. & Varga, R. A. (2021). *New J. Chem.* **45**, 1020–1028.

Wan, J., Li, F., Zeng, W.-L., Li, J. & Bi, S. (2007). *Acta Cryst.* E**63**, o3989.

Wang, W. & Mei, Z.-H. (2009). *Acta Cryst.* E**65**, o357.

supporting information

Acta Cryst. (2024). E**80** [https://doi.org/10.1107/S2056989024010594]

Crystal structure, Hirshfeld surface analysis, DFT and molecular docking studies of ethyl 5-amino-2-bromoisonicotinate

Harish Kumar Mahadevaiah, Harishkumar Shivanna, Anil Kumar Hanumaiah, Devarajegowda Hirehalli Chikkegowda and Palakshamurthy Bandrehalli Siddagangaiah

Computing details

Ethyl 5-amino-2-bromopyridine-4-carboxylate

Crystal data

$C_8H_9BrN_2O_2$
$M_r = 245.08$
Monoclinic, $P2_1/c$
$a = 4.1538$ (9) Å
$b = 8.9978$ (16) Å
$c = 25.487$ (5) Å
$\beta = 92.468$ (7)°
$V = 951.7$ (3) Å^3
$Z = 4$
$F(000) = 488$
$D_x = 1.710$ Mg m^{-3}
Mo $K\alpha$ radiation, $\lambda = 0.71073$ Å
Cell parameters from 2367 reflections
$\theta = 2.5$–29.0°
$\mu = 4.29$ mm^{-1}
$T = 567$ K
Prism, pale yellow
0.32 × 0.27 × 0.21 mm

Data collection

Bruker SMART APEXII CCD diffractometer
Radiation source: fine-focus sealed tube
Graphite monochromator
Detector resolution: 0.97 pixels mm^{-1}
φ and Ω scans
Absorption correction: multi-scan (SADABS; Krause *et al.*, 2015)
$T_{min} = 0.225$, $T_{max} = 0.401$
21643 measured reflections
2353 independent reflections
1910 reflections with $I > 2\sigma(I)$
$R_{int} = 0.037$
$\theta_{max} = 28.3°$, $\theta_{min} = 2.8°$
$h = -5 \rightarrow 5$
$k = -11 \rightarrow 11$
$l = -33 \rightarrow 33$

Refinement

Refinement on F^2
Least-squares matrix: full
$R[F^2 > 2\sigma(F^2)] = 0.032$
$wR(F^2) = 0.069$
$S = 1.04$
2353 reflections
126 parameters
0 restraints
0.12 constraints
Primary atom site location: structure-invariant direct methods
Secondary atom site location: difference Fourier map
Hydrogen site location: mixed
H atoms treated by a mixture of independent and constrained refinement
$w = 1/[\sigma^2(F_o^2) + (0.0216P)^2 + 0.6676P]$ where $P = (F_o^2 + 2F_c^2)/3$
$(\Delta/\sigma)_{max} = 0.001$
$\Delta\rho_{max} = 0.53$ e Å^{-3}
$\Delta\rho_{min} = -0.45$ e Å^{-3}

Special details

Geometry. All esds (except the esd in the dihedral angle between two l.s. planes) are estimated using the full covariance matrix. The cell esds are taken into account individually in the estimation of esds in distances, angles and torsion angles; correlations between esds in cell parameters are only used when they are defined by crystal symmetry. An approximate (isotropic) treatment of cell esds is used for estimating esds involving l.s. planes.

Fractional atomic coordinates and isotropic or equivalent isotropic displacement parameters (Å²)

	x	*y*	*z*	U_{iso}*/U_{eq}
Br1	0.50981 (7)	0.23668 (3)	0.33291 (2)	0.06255 (12)
O1	0.6756 (4)	0.71953 (17)	0.44789 (6)	0.0519 (4)
O2	0.4245 (5)	0.91607 (19)	0.41176 (7)	0.0678 (5)
N2	0.0811 (7)	0.8705 (3)	0.31867 (10)	0.0679 (7)
C1	0.3910 (5)	0.6820 (2)	0.36780 (8)	0.0389 (4)
C2	0.1949 (6)	0.7303 (2)	0.32486 (8)	0.0451 (5)
C3	0.1106 (6)	0.6220 (3)	0.28677 (9)	0.0511 (6)
H3	−0.019460	0.651860	0.258076	0.061*
N1	0.2016 (5)	0.4817 (2)	0.28864 (7)	0.0480 (5)
C4	0.3867 (5)	0.4403 (2)	0.32981 (8)	0.0419 (5)
C5	0.4870 (5)	0.5336 (2)	0.36960 (8)	0.0414 (5)
H5	0.617469	0.498569	0.397470	0.050*
C6	0.4947 (6)	0.7863 (3)	0.41030 (8)	0.0455 (5)
C7	0.7917 (7)	0.8112 (3)	0.49174 (9)	0.0558 (6)
H7A	0.612483	0.860208	0.507725	0.067*
H7B	0.938171	0.886598	0.479721	0.067*
C8	0.9601 (8)	0.7121 (4)	0.53018 (11)	0.0737 (8)
H8A	1.039906	0.769478	0.559719	0.111*
H8B	0.812758	0.638136	0.541835	0.111*
H8C	1.137029	0.664411	0.513954	0.111*
H2A	−0.018 (6)	0.889 (3)	0.2911 (12)	0.064 (8)*
H2B	0.141 (7)	0.934 (3)	0.3432 (12)	0.067 (9)*

Atomic displacement parameters (Å²)

	U^{11}	U^{22}	U^{33}	U^{12}	U^{13}	U^{23}
Br1	0.07039 (19)	0.04411 (15)	0.0714 (2)	0.00444 (12)	−0.01747 (13)	−0.01644 (12)
O1	0.0718 (11)	0.0421 (8)	0.0399 (8)	0.0006 (7)	−0.0200 (7)	−0.0075 (7)
O2	0.1044 (15)	0.0396 (9)	0.0572 (11)	0.0078 (9)	−0.0225 (10)	−0.0068 (8)
N2	0.102 (2)	0.0467 (12)	0.0519 (14)	0.0056 (12)	−0.0313 (13)	0.0091 (10)
C1	0.0475 (12)	0.0382 (10)	0.0304 (10)	−0.0056 (9)	−0.0048 (9)	0.0015 (8)
C2	0.0559 (13)	0.0426 (11)	0.0359 (11)	−0.0058 (10)	−0.0073 (9)	0.0083 (9)
C3	0.0625 (15)	0.0560 (14)	0.0334 (11)	−0.0075 (11)	−0.0139 (10)	0.0050 (10)
N1	0.0569 (12)	0.0513 (11)	0.0349 (9)	−0.0085 (9)	−0.0090 (8)	−0.0041 (8)
C4	0.0460 (12)	0.0399 (11)	0.0394 (11)	−0.0056 (9)	−0.0026 (9)	−0.0042 (9)
C5	0.0488 (12)	0.0414 (11)	0.0331 (10)	−0.0033 (9)	−0.0090 (9)	0.0005 (8)
C6	0.0589 (14)	0.0401 (11)	0.0367 (11)	−0.0036 (10)	−0.0069 (10)	−0.0005 (8)
C7	0.0683 (16)	0.0557 (14)	0.0418 (12)	−0.0052 (12)	−0.0159 (11)	−0.0167 (11)
C8	0.080 (2)	0.091 (2)	0.0478 (15)	−0.0032 (17)	−0.0203 (14)	−0.0065 (14)

Geometric parameters (Å, º)

Br1—C4	1.903 (2)	C3—N1	1.318 (3)
O1—C6	1.335 (3)	C3—H3	0.9300
O1—C7	1.454 (2)	N1—C4	1.327 (3)
O2—C6	1.204 (3)	C4—C5	1.368 (3)
N2—C2	1.354 (3)	C5—H5	0.9300
N2—H2A	0.82 (3)	C7—C8	1.478 (4)
N2—H2B	0.87 (3)	C7—H7A	0.9700
C1—C5	1.393 (3)	C7—H7B	0.9700
C1—C2	1.405 (3)	C8—H8A	0.9600
C1—C6	1.483 (3)	C8—H8B	0.9600
C2—C3	1.409 (3)	C8—H8C	0.9600
C6—O1—C7	117.00 (18)	C1—C5—H5	120.5
C2—N2—H2A	117 (2)	O2—C6—O1	123.0 (2)
C2—N2—H2B	115.9 (19)	O2—C6—O1	123.0 (2)
H2A—N2—H2B	127 (3)	O2—C6—C1	125.0 (2)
C5—C1—C2	118.54 (19)	O2—C6—C1	125.0 (2)
C5—C1—C6	120.56 (19)	O1—C6—C1	112.08 (19)
C2—C1—C6	120.9 (2)	O1—C7—C8	107.4 (2)
N2—C2—C1	124.5 (2)	O1—C7—H7A	110.2
N2—C2—C3	119.3 (2)	C8—C7—H7A	110.2
C1—C2—C3	116.2 (2)	O1—C7—H7B	110.2
N1—C3—C2	125.1 (2)	C8—C7—H7B	110.2
N1—C3—H3	117.4	H7A—C7—H7B	108.5
C2—C3—H3	117.4	C7—C8—H8A	109.5
C3—N1—C4	116.92 (19)	C7—C8—H8B	109.5
N1—C4—C5	124.2 (2)	H8A—C8—H8B	109.5
N1—C4—Br1	116.65 (15)	C7—C8—H8C	109.5
C5—C4—Br1	119.19 (16)	H8A—C8—H8C	109.5
C4—C5—C1	119.1 (2)	H8B—C8—H8C	109.5
C4—C5—H5	120.5		
C5—C1—C2—N2	179.0 (2)	C6—C1—C5—C4	179.9 (2)
C6—C1—C2—N2	−1.2 (4)	C7—O1—C6—O2	−0.6 (4)
C5—C1—C2—C3	0.2 (3)	C7—O1—C6—O2	−0.6 (4)
C6—C1—C2—C3	−180.0 (2)	C7—O1—C6—C1	180.0 (2)
N2—C2—C3—N1	−179.0 (3)	C5—C1—C6—O2	179.6 (2)
C1—C2—C3—N1	−0.1 (4)	C2—C1—C6—O2	−0.2 (4)
C2—C3—N1—C4	0.1 (4)	C5—C1—C6—O2	179.6 (2)
C3—N1—C4—C5	−0.2 (3)	C2—C1—C6—O2	−0.2 (4)
C3—N1—C4—Br1	178.77 (18)	C5—C1—C6—O1	−1.0 (3)
N1—C4—C5—C1	0.3 (4)	C2—C1—C6—O1	179.1 (2)
Br1—C4—C5—C1	−178.67 (16)	C6—O1—C7—C8	175.2 (2)
C2—C1—C5—C4	−0.2 (3)		

Hydrogen-bond geometry (Å, º)

D—H···*A*	*D*—H	H···*A*	*D*···*A*	*D*—H···*A*
N2—H2*B*···O2	0.87 (3)	2.07 (3)	2.746 (3)	133 (2)
C5—H5···O1	0.93	2.37	2.694 (3)	100 (1)
N2—H2*A*···N1^{i}	0.82 (3)	2.30 (3)	3.096 (3)	166 (3)

Symmetry code: (i) −*x*, *y*+1/2, −*z*+1/2.